IOP Publishing Journal of Physics D: Applied Physics
J. Phys. D: Appl. Phys. **40** (2007) 5571–5579 doi:10.1088/0022-3727/40/18/010

Spectral investigation of a large-area 2D silicon photonic crystal slab for mid-IR radiation

L Prodan[1,2,7], P Groß[1,3], R Beigang[4], L Kuipers[5,6] and K-J Boller[1]

[1] Laser Physics and Nonlinear Optics Group, Department of Science and Technology, and MESA+ Research Institute, University of Twente, PO Box 217, Enschede 7500 AE, The Netherlands
[2] Laser Applicatie Centrum, University of Twente, PO Box 217, Enschede 7500 AE, The Netherlands
[3] Optical Technologies Group, Institute of Applied Physics, Westfälische Wilhelms-Universität Münster, Corrensstr. 2-4, Münster 48149, Germany
[4] Fachbereich Physik, Technische Universität Kaiserslautern, Erwin-Schrödinger-Str. 46, 67663 Kaiserslautern, Germany
[5] Optical Techniques Group, Department of Science and Technology, and MESA+ Research Institute, University of Twente, PO Box 217, Enschede 7500 AE, The Netherlands
[6] Center for Nanophotonics, FOM—Institute for Atomic and Molecular Physics AMOLF, Kruislaan 407, Amsterdam 1098 SJ, The Netherlands

E-mail: L.Prodan@tnw.utwente.nl

Received 30 March 2007, in final form 30 July 2007
Published 30 August 2007
Online at stacks.iop.org/JPhysD/40/5571

Abstract
A two-dimensional silicon photonic crystal (PhC), which is designed to provide a modified dispersion for photon energies of less than half of the electronic band gap of silicon, and which has been fabricated by laser interference lithography (LIL), is studied by angular dependent infrared reflectivity measurements. The resonance features, which we observe in the polarized reflectivity spectra, and which arise from resonant coupling of the infrared radiation to the leaky modes, are used to derive the probed leaky modes' quality factor of the PhC fabricated by LIL. We also present photonic band structure calculations to reveal the bandgaps of the guided modes.

(Some figures in this article are in colour only in the electronic version)

1. Introduction

Photonic crystals (PhCs) are composite materials, for which a large, periodic variation of the dielectric function leads to a dramatic change of the propagation properties of light [1]. These crystals can be designed and manufactured to offer specific propagation properties, as desired to achieve, e.g. control of spontaneous emission [2], localization of light [3] or propagation along arbitrary paths [4]. Besides their remarkable linear properties, out of which the above mentioned possibilities arise, such crystals also promise to possess interesting nonlinear properties, many of which are based on altering the index of refraction through the third-order optical nonlinearity, $\chi^{(3)}$, and which can lead to the possibility of tuning the transmission wavelength [5, 6] or rapidly switching the transmission of PhCs [7] or designing the spatial and temporal shape of a propagating pulse. The latter can be used to create spatial or temporal solitons, or a combination of both, which is often termed light bullets [8, 9].

However, despite the high potential, the nonlinear properties of PhCs are by far less well investigated and understood than the linear properties. Previous demonstrations of third-order nonlinear effects in PhCs have been dominantly accompanied by unwanted linear (absorption) and resonant third-order nonlinear effects (two-photon losses), which make the observation of the aimed effects difficult. A first step towards the application of PhCs to nonlinear propagation effects would be the transition to the infrared spectral region. Under such circumstances, i.e. when light with photon energies

[7] Author to whom any correspondence should be addressed.

of less than half the electronic bandgap of Si (1.1 eV, corresponding to a wavelength of 2.1 μm) propagates through a Si PhC with a designed dispersion for MIR propagation, two-photon losses will be strongly reduced. As a result, the residual material effects could thus be neglected, and the unaltered properties of the structure could be studied.

Leonard and colleagues have demonstrated band-edge tuning using macroporous silicon, where the near-infrared wavelength of 1.9 μm used to probe the PhC modes helped avoiding linear absorption [6], but where the photon energy was still high enough to allow two-photon absorption. A designed dispersion in the mid-infrared spectral region, as would be desirable for the unaltered observation of third-order nonlinear effects, has not been demonstrated until today, despite the anticipated advantages when using MIR light, and despite the propagation properties of visible and near-infrared light with frequencies relevant for telecommunication being designed and realized almost routinely.

Here, we present the first, linear characterization of a PhC, which has been designed to enable the intended nonlinear experiments, and which has been fabricated using laser interference lithography (LIL) [10]. In this contribution, we determine the dispersion curves (optical frequency as a function of wave vector) in the range from 1.9 to 2.8 μm by means of reflectance spectroscopy at oblique incidence. We determine the quality factors of these leaky modes of the PhC from the bandwidth of the observed resonance features, which is, to the authors' knowledge, the first report about the quality factors of a PhC sample manufactured using LIL. Finally, we use the experimentally obtained data to reconstruct the band structure, which indicates the existence of a bandgap and of the dispersion required for nonlinear experiments in the desired MIR frequency region.

2. Sample design and preparation

Recently, we have designed a PhC such that it should enable the study of nonlinear effects in the desired MIR wavelength range. Specifically, it should offer the possibility of generating both spatial and temporal solitons by exploiting the third-order nonlinear Kerr effect. The generation of such spatio-temporal Kerr-solitons or light bullets has been investigated theoretically [11]. For this purpose, several requirements must be fulfilled: first, the material in which the light propagates needs to show a sufficiently high *positive* Kerr-coefficient, such that diffraction can be balanced by Kerr-self-focusing. Furthermore, for spatial solitons to form, the medium is required to have 2D or slab geometry, because in 3D or bulk media Kerr-self-focusing is believed to lead to transverse instabilities and eventually to beam break-up [12]. Second, a temporal soliton can form due to the positive Kerr effect, if it travels through a medium with *anomalous* dispersion, i.e. through a medium where the long-wavelength part of the light falls back to the trailing pulse edge [13]. Anomalous dispersion can be realized, e.g. in a PhC in close vicinity to either a stop gap or a photonic bandgap, i.e. to a frequency interval within which the propagation of light is not possible. In summary, in order to investigate the formation of spatio-temporal Kerr-solitons, a PhC slab of highly Kerr-nonlinear material is required, which shows anomalous dispersion in the MIR spectral region around 2.6 μm.

The PhC designed for this purpose is based on silicon, which offers a high, positive Kerr-nonlinearity [14], and which has an electronic bandgap energy of 1.1 eV, such that illumination with light of a wavelength longer than 2.1 μm (equivalent to an energy of 0.55 eV) should enable experiments with strongly reduced two-photon absorption. The structure is sketched schematically in the upper left graph of figure 1. It is based on a PhC slab design, i.e. a 0.5 μm thick film of silicon on a 3 μm thick SiO_2 layer (silicon on insulator, SOI), which separates the waveguide slab from the underlying Si wafer (not shown in figure 1). In such a PhC slab, standard waveguiding confines the light to the PhC plane with a higher index of refraction, i.e. to the silicon layer with $n \approx 3.4$ at $\lambda = 2.6\,\mu$m (compared with SiO_2 with $n \approx 1.4$ on one side and to air on the other side). The dispersion of in-plane wave vectors is determined by periodic refractive index modulation in the silicon plane. Previously, we have calculated that a square lattice array of air holes with a diameter of around 0.8 μm and with a lattice constant of 1 μm should offer the required anomalous dispersion for wavelengths around 2.5 μm. The upper right part of figure 1 shows the irreducible Brillouin zone (IBZ) corresponding to this square lattice with the standard notation of the high-symmetry points, Γ, X and M.

The crystal has been fabricated using a commercially available SOI bulk wafer [15] with LIL [16]. In comparison with other, conventional techniques to fabricate 2D PhCs, LIL is rather simple and cost-effective, and it allows the production of large-area 2D PhCs with high periodicity. For example, e-beam lithography (EBL) [17] or a focused ion beam (FIB) [18] are sequential techniques, which are relatively slow and prone to drift. Deep-UV lithography [19] can be used to fabricate 2D PhCs on a larger scale, but it requires costly equipment like, for example, a deep-UV laser for mask fabrication and a waver stepper. The here implemented technique LIL, on the other hand, enables the fabrication of large-area 2D PhCs with a well-defined periodicity following the interference pattern of a standard UV laser. The interference pattern leads to a limited choice of 2D structures, which can then be combined with a sequential writing technique, such as FIB, to add defects to a pre-made periodic structure [10].

The fabrication of the PhC slab under investigation using LIL and a negative photoresist is described in more detail in [16]. In order not to alter the properties of the planar waveguide, the etching process has been carefully controlled, such that the holes do not penetrate the SiO_2 layer. The latter has been verified with a scanning electron microscope (SEM) image of the fabricated structure. A second (SEM) image, which is shown in the lower part of figure 1, has been used to verify the 1 μm lattice constant of the square lattice and the high periodicity within the whole $1 \times 1\,cm^2$ surface of the PhC. We believe that this exceptionally large surface of the PhC is of particular advantage for the study presented in the following, because the result of a single measurement, where a large portion of the PhC is illuminated simultaneously, is equivalent to an average over a number of measurements over a smaller surface.

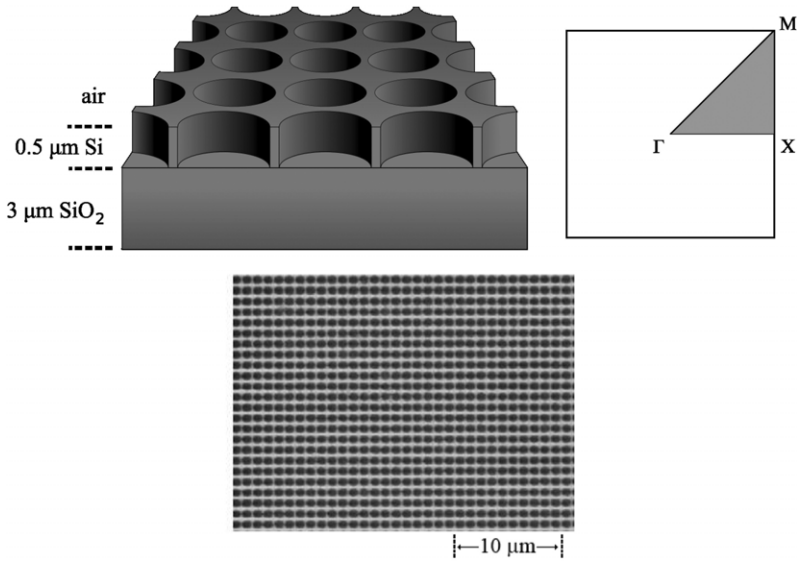

Figure 1. Upper left: schematic of the 2D PhC consisting of a square lattice of holes in silicon. Upper right: corresponding irreducible Brillouin zone with the high-symmetry points Γ, X and M. The angle between the Γ–X and Γ–M crystal symmetry direction is 45°. Lower: SEM micrograph of the PhC, top view. The round holes appear slightly elliptic due to a difference in vertical versus horizontal resolution (compare also with figure 3 in [16]).

3. Experimental setup

The dispersion of the PhC slab is probed by angle- and wavelength-resolved reflectivity measurements. This technique is based on the observation of resonant coupling, when the in-plane component of the incident wavevector matches the wavevector of the photonic bands, and has been applied to PhC slabs earlier [20–22]. Because only the projection of the wavevector can be coupled to the PhC modes, this coupled wavevector is reduced with respect to the wavevector of the light in surrounding air by a factor $\sin(\theta)$, where θ is the angle of incidence. Thus, the magnitude of the component of the wavevector parallel to the surface can never match that of a guided mode, as the guided modes lie below the so-called light line. This excludes the direct probing of the dispersion of guided modes via simple reflection measurements. Rather one expects a coupling only to the leaky (or quasi-guided) modes. In the work described in [20], a high-index prism has been used to increase the range of accessible energy-wavevector combinations. In our work, we follow a different and less involved approach where the dispersion of the leaky modes is probed experimentally.

Preliminary calculations[8] have shown, that for a mapping of the dispersion curves of the leaky modes of our photonic structure, we require a light source that covers the range of photon energies from 0.44 to 0.65 eV, i.e. the wavelength range from 1.9 to 2.8 μm. Additionally, to provide the proper wave vector range, the angle of incidence, θ, must be adjustable from 10° to 70°. The divergence of the incident beam is then the limiting factor for the precision: a distribution over a range of angles of incidence will result in a distribution over a range of projected wavevectors and will thus ultimately limit the resolution, with which the coupled wavevector can be determined, and thus the contrast between spectral features in the reflectivity spectra. Furthermore, the cross section of the beam should be adapted to evenly illuminate a large portion of the PhC structure, such that a single measurement represents the equivalent of averaging over a wide surface area and thus enhance the obtainable signal-to-noise ratio.

To realize a light source with a small beam divergence and tunable spectral range, we employ a broad-bandwidth light source and select appropriate beam shaping, wavelength-selection and polarization optics. The resulting setup is shown schematically in figure 2. As a broad-bandwidth light source, we use a 250 W quartz tungsten halogen (QTH) lamp (Oriel 66995), driven by a stabilized current supply. This white-light source emits a spectral power of more than 3 mW nm^{-1} over the desired wavelength range from 1.9 to 2.8 μm. The white light is spectrally filtered using a 300 mm monochromator (Hilger and Watts) with a grating of 750 lines mm^{-1} and with blazing for MIR wavelengths. Using a wire-grid polarizer, the polarization is chosen to be either parallel or perpendicular to the plane of reflection, i.e. we choose either transversal-electric (TE) or transversal-magnetic (TM) polarized light. Finally, a high-pass optical filter is used to remove light transmitted through the monochromator in higher order.

With this experimental setup, we generate a wavelength tunable mid-IR light beam, which illuminates the PhC sample with the following characteristics: the power in front of the sample is approximately 2 nW, with a spectral bandwidth of 5 nm. The beam divergence is estimated to be 3°, which translates into a wavevector error ranging from less than 30% for the smallest angle of incidence, $\theta = 10°$, to less than 2% for $\theta = 70°$. The beam cross section is of rectangular shape with 2 mm×5 mm, such that, even at high angle of incidence (up to 70°) the projection of the beam cross section is entirely within the 100 mm^2 area of the sample. This represents a compromise between the wave vector resolution, the spectral resolution, and the signal-to-noise ratio.

[8] The calculations were carried out using a 30-day trial version of the DiffractMOD™ software packet. DiffractMOD™ is a registered trademark of the Rsoft Design Group Inc.

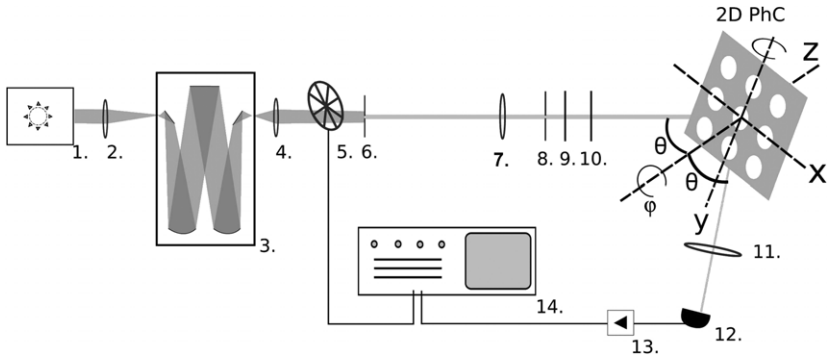

Figure 2. Experimental setup for specular reflectivity measurements. The individual components are: 1, QTH light source; 2, lens; 3, monochromator; 4, lens; 5, optical chopper; 6, slit; 7, lens; 8, pinhole; 9, low-pass filter; 10, polarizer; 11, lens; 12, detector; 13, amplifier; 14, lock-in amplifier.

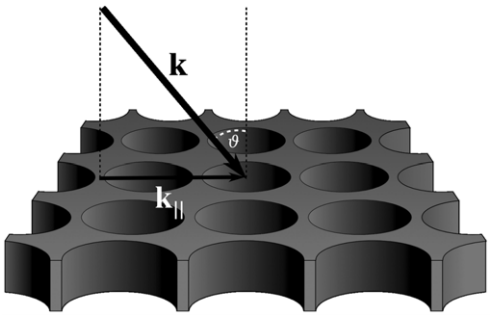

Figure 3. Schematic representation of the projection of the k vector of the incident light onto the plane of the slab waveguide. The in-plane wave vector is labelled k_{II} and determined by the angle θ between the incident light and the normal on the plane.

The sample is mounted on a rotation stage and rotated around the surface normal, such that the direction of the in-plane wave vector of the incident light, i.e. the projection of the wave vector on the sample surface, is along one of the two symmetry directions Γ–M and Γ–X of the quadratic lattice, i.e. along the directions connecting the symmetry points Γ and M, and Γ and X, respectively. The desired orientation is verified by inspecting the mounted sample with a microscope. A second rotation stage allows the variation of the angle of incidence θ, as required for changing the in-plane component of the incident wavevector figure 3.

The light reflected off the PhC surface is weak, of only nW power level, and it is in a spectral region where detectors with low noise and high quantum efficiency are not readily available. Nevertheless, even small changes in reflectivity can indicate coupling to a leaky mode. Therefore, to enable a high signal-to-noise ratio, a sensitive MIR detector is combined with a powerful and low-noise amplifier as follows. After reflection off the surface of the sample, the light passes a rotating-disc optical chopper with the chopping frequency set to 3.5 kHz, and is projected using a lens of 100 mm focal length on the detector. As a detector for the MIR radiation, a photoconductive PbS detector is used (OEC GmbH, model A5-0-3), which is carefully protected from surrounding light as well as from stray light originating from the white-light QTH source. To maximize detector efficiency, a bias voltage of 110 V is applied. For a high signal-to-noise ratio, a differential pre-amplifier is employed, followed by an integrating amplifier, which, by eliminating the dc component of the signal, ensures that the differential amplifier operates in the linear regime. The circuit is designed similar to the one described in [23]. The amplified detector signal is processed using a lock-in amplifier (Princeton Applied Research Corp., Model 129A). The described detection scheme enables a signal-to-noise ratio of 25 at nW power level in the MIR spectral region and is thus suitable to record even weak changes in reflectivity from the PhC surface.

4. Results and discussion

4.1. Specular reflectivity spectra

Specular reflectivity spectra are obtained along the Γ–M symmetry direction, and along the Γ–X symmetry direction for two perpendicular polarizations of incident light, and for angles of incidence varying between $\theta = 10^\circ$ and 70°. The spectra of the reflected light were normalized to the spectra of the QTH lamp, obtained by placing the detector on the sample position. In figure 4, the reflectivity of the PhC slab along the Γ–M symmetry direction is displayed as a function of wavelength by the black curves, for the two cases when the light was TE polarized (in plane of reflection, figure 4(*a*)), and when the light was TM polarized (perpendicular to the plane of reflection, figure 4(*b*)). In both figures, the angle of incidence, θ, increases from bottom ($\theta = 10^\circ$) to top ($\theta = 70^\circ$).

Both sets of spectra show sharp features superimposed on a background, part of which can have originated from residual light sources in the room and from stray light of the QTH light source. The sharp features shift in wavelength with the variation of the incidence angle by more than 200 nm. Upon a comparison of the two graphs in figures 4(*a*) and (*b*), it is found that the spectra recorded for TE polarization clearly differ from those recorded for TM polarization, and that there is no polarization mixing evident.

In order to verify the design parameters of the crystal, such as hole radius and layer thickness, which are required to calculate the guided modes band structure and to prepare the nonlinear experiments, we have compared the measured reflectivity spectra with theoretical ones. The theoretical reflectivity spectra are calculated using a commercially available simulation tool, which solved the Maxwell equations by rigorous coupled wave analysis[8], and which takes into

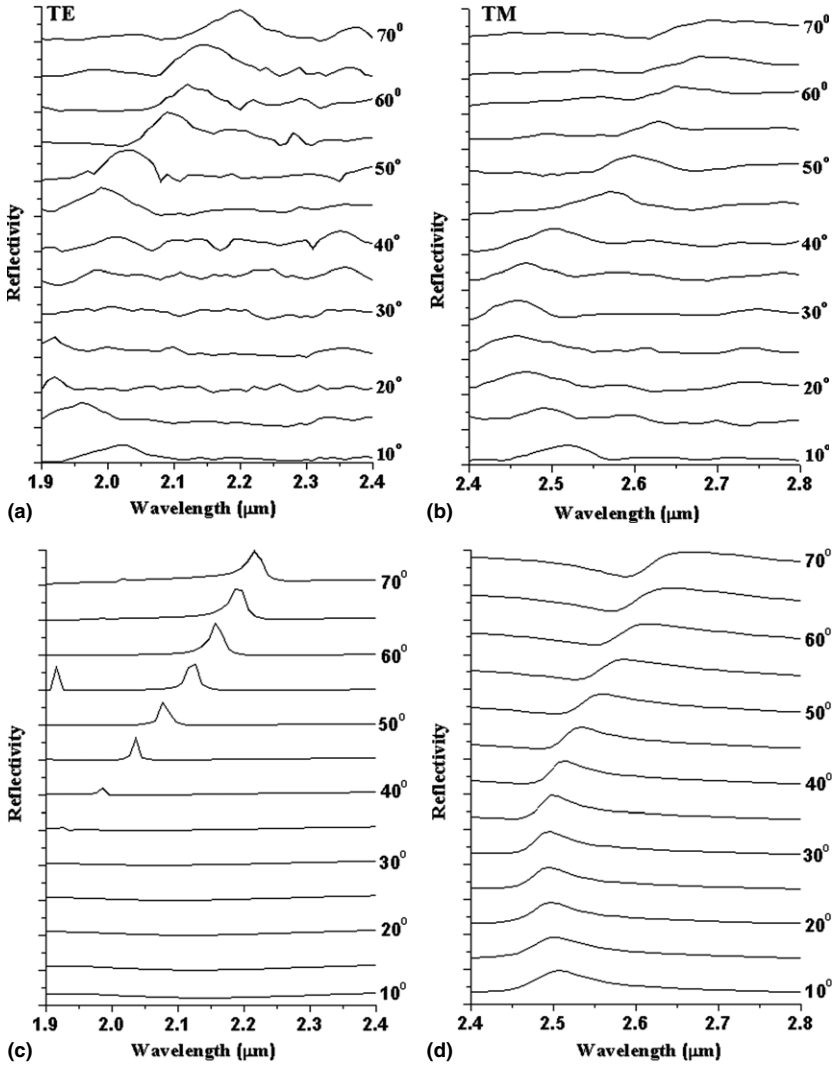

Figure 4. Reflectivity of the PhC slab as a function of wavelength for propagation along the Γ–M symmetry direction. The distance between the large ticks on the vertical axes corresponds to absolute reflectivities between zero and unity for each trace. (*a*) Measured reflectivity for TE polarized and (*b*) for TM polarized light, (*c*) calculated reflectivity for TE polarized and (*d*) for TM polarized light. The curves are vertically shifted for clarity; from bottom to top, the angle of incidence increases from $\theta = 10^\circ$ to 70°.

account Fresnel reflection at the layer interfaces. The result for Γ–M symmetry direction is shown in figures 4(*c*) and (*d*), for TE and for TM polarized incident light, respectively.

Measurements and calculations are also performed along the Γ–X symmetry direction for both polarizations. The measured spectra are displayed in figures 5(*a*) (TE polarization) and (*b*) (TM polarization), while the calculated spectra are shown in figures 5(*c*) and (*d*) for TE and TM polarized light, respectively. It can be seen that calculated and measured reflectivities are comparable. Again, the spectra display distinct features, which also shift in wavelength, as the angle of incidence is varied. In figures 4(*c*) and (*d*) and figures 5(*c*) and (*d*) one can also see some slowly varying, background-like features (e.g. in figure 4(*c*) at 10°, or in figure 5(*d*) at 40° around 2 μm) which are probably due to broadband Fresnel reflection or broad Fabry Perot fringes from the SiO_2 layer underneath the periodic structure. For both polarizations and for both symmetry directions, a hole radius of 0.4 μm and a Si layer thickness of 0.5 mm were found to yield the best fit with the measured spectra. As a consequence, the parameters so obtained are used to complement the design parameters of periodicity of 1 μm and the material refractive indices in order to calculate the complete guided modes band structure, which is presented in section 4.4.

4.2. Line shapes of observed features

A closer investigation reveals that the features possess different line shapes, such as maxima, minima, and dispersive (asymmetric) forms. Similar asymmetric line shapes have been observed before for the case of one-dimensional structures [24] as well as for two-dimensional triangular [21] and square lattices [22]. In [21], these dispersive line shapes have been explained by a phase shift of the reflected light when coupling to a leaky mode occurs, and the dependence of the shape of the observed features on the depth of the holes structure could be verified by simulation of the reflectivity. It is evident, however, that these differences in line shape hamper a direct extraction of the centre wavelength and the linewidth of the probed leaky modes, which is crucial for the characterization

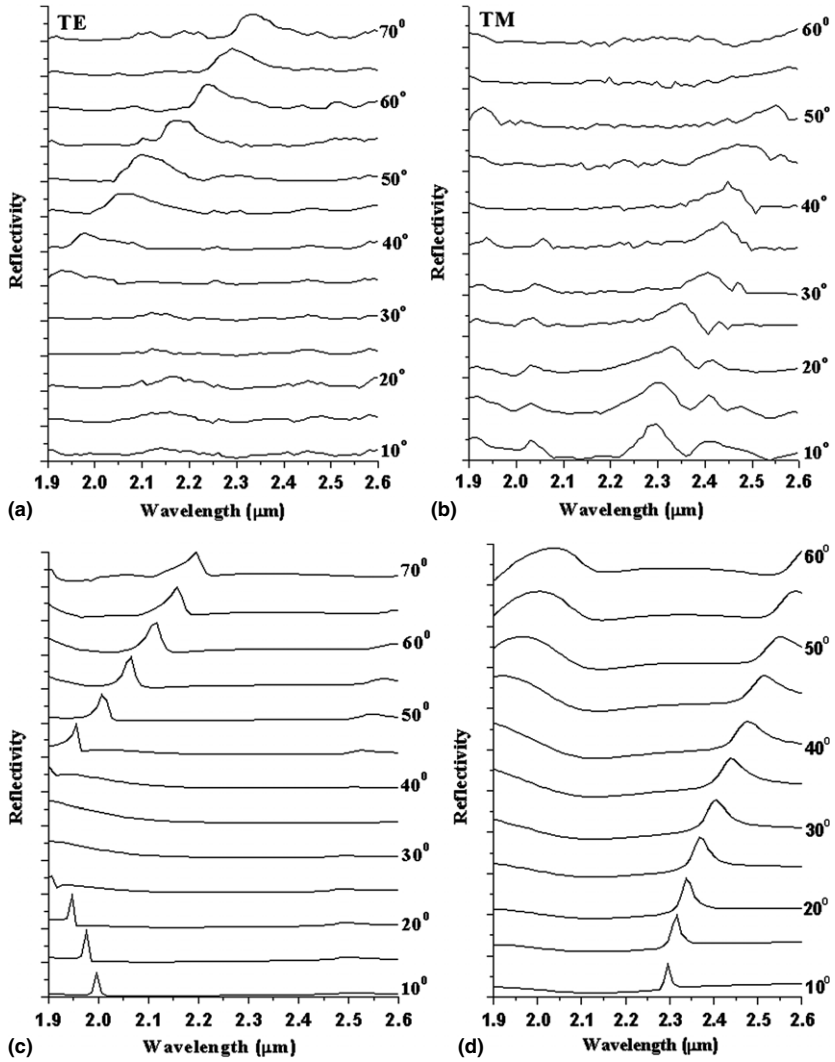

Figure 5. Reflectivity of the PhC slab as a function of wavelength for propagation along the Γ–X symmetry direction. Measured reflectivity (*a*) for TE polarized and (*b*) for TM polarized light. Calculated reflectivity (*c*) for TE polarized and (*d*) for TM polarized light. The curves are vertically shifted for clarity; from bottom to top, the angle of incidence increases from $\theta = 10^\circ$ to 70° (*a*) and from 10° to 60° (*b*).

of a PhC. Therefore, to enable an accurate determination of the named values, we adopt an expression to describe the line shapes, which has been derived in the classical Fano paper from 1961 [25], and which has been used before to describe reflectivity features of PhCs [20, 22].

With the energy $E = \hbar\omega$ of the incident photons, the energy of the resonant modes $E_0 = \hbar\omega_0$ with centre frequency ω_0, and a linewidth of the resonant mode $\Gamma = \hbar\gamma$, we obtain the reduced energy variable ε in analogy to equation (19) of [25]:

$$\varepsilon = \frac{\hbar\omega - \hbar\omega_0}{\frac{1}{2}\hbar\gamma}. \tag{1}$$

The line shape of the features can then be expressed by (compare equation (21) of [25]):

$$F(\omega) = F_0 \frac{(q+\varepsilon)^2}{1+\varepsilon^2} = F_0 \cdot \left[1 + \frac{q^2 - 1 + 4q(\omega-\omega_0)/\gamma}{1 + 4(\omega-\omega_0)^2/\gamma^2}\right]. \tag{2}$$

Here, F_0 is oscillator strength, while the parameter q may assume values between -1 and $+1$ and determines the shape of the resonance. The parameter q can be regarded as a coupling parameter of the incident photons to the leaky modes of the PhC (compare equation (22) of [25]).

Equation (2) is fitted to the reflectivity features, which can be identified in the experimental data, with the centre frequency, the linewidth of the feature, and the q-parameter as fitting parameters (two additional fit parameters are an offset and a scaling factor which are not supposed to be of much relevance for the centre frequency, linewidth and q-parameter fits). In some of the spectra, several, partially overlapping features can be observed. To obtain the centre frequencies and linewidths of such features, we apply a linear combination of two or more of such line shapes. We note, however, that such a superposition can be applied only, if the two resonances do not couple, for in that case the measured line shape may differ substantially from a mere superposition of the two resonance features [26]. As an example, figure 6 displays the experimental data obtained for the Γ–X symmetry direction, TM polarization, and for an angle of incidence of 10° (measured points displayed as squares), together with three Fano fits (solid lines, derived from equation (2)). The fits

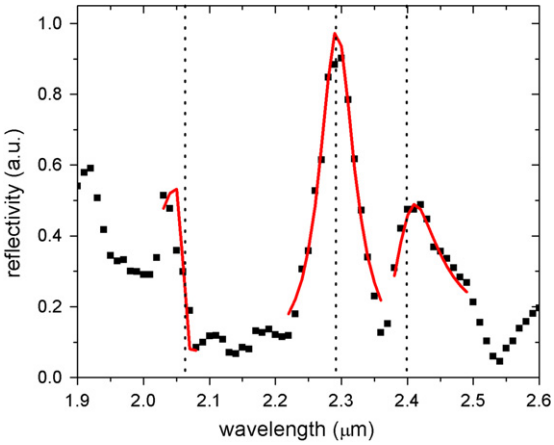

Figure 6. Example of a measured reflectivity spectrum with Fano-like line shapes. Squares: measured reflectivity for the Γ–X symmetry direction, TM polarization and 10° angle of incidence as a function of wavelength. Solid lines: Fano-line shapes fitted to three distinct reflectivity features. Dotted vertical lines: centre wavelengths of the Fano-line shapes.

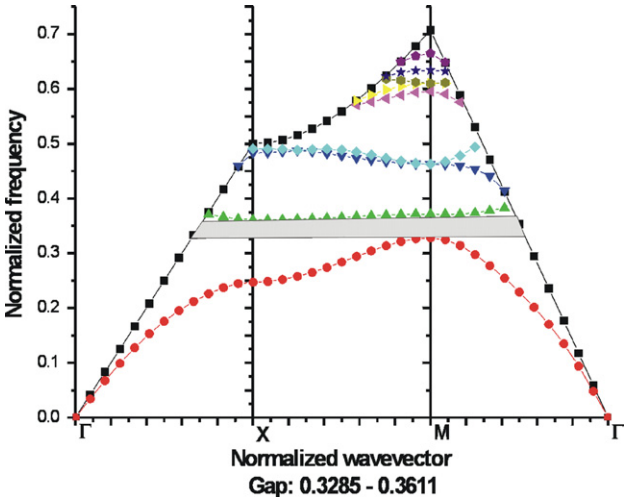

Figure 7. Calculated dispersion curves of the guided modes for TE polarized light. Guided modes (coloured symbols) are plotted under the light line (black squares), revealing a bandgap (grey bar) for normalized frequencies around 0.36 (grey bar).

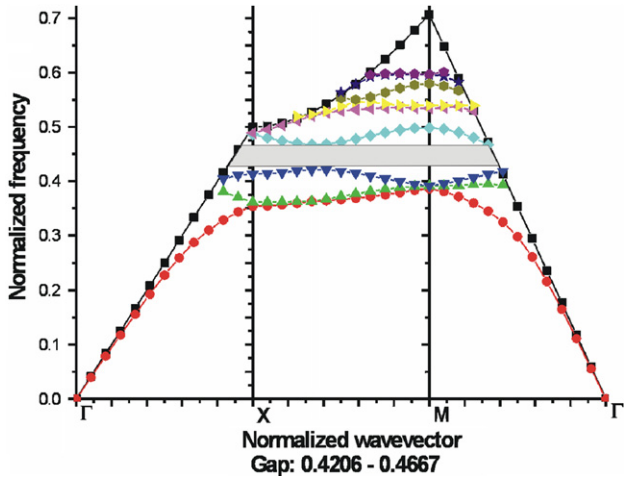

Figure 8. Calculated dispersion curves of the guided modes for TM polarized light. Guided modes (coloured symbols) are plotted under the light line (black squares), revealing a bandgap (grey bar) for normalized frequencies around 0.44 (grey bar).

yield, in this example, features with centre wavelengths of 2.06, 2.24 and 2.29 μm (indicated by vertical dotted lines). This example demonstrates the suitability of the Fano function equation (2) to describe the measured line shapes in the reflectivity spectra. In the following, we present the results obtained by fitting the described formula to our experimental specular reflectivity spectra, i.e. the bandwidth and the centre frequency of the features observed in the spectra.

4.3. Quality factor

The quality factor, Q, of a photonic structure is a measure for the lifetime of a PhC mode. The lifetime of the investigated leaky modes is, on the one hand, intrinsically limited by radiation losses. On the other hand, fabrication imperfections such as irregularities regarding the hole size, hole roundness and hole displacement (i.e. an erratious periodicity) can further lower the lifetime and thus influence the spectral characteristics and, specifically, the width of the Fano resonances. The measurement of Q would thus give a valuable first indication of the quality, i.e. the regularity of a structure that can be expected from this novel manufacturing method LIL. In this contribution, we determine the quality factor Q of the investigated leaky modes from the ratio of the centre frequency and the linewidth of the measured features, $Q = (\omega_0/\gamma)$, both being obtained from fitting the Fano-line shape to the measured reflectivity spectra.

The quality factor is calculated for each of the reflectivity features, which could be identified in the measurements presented in figures 4 and 5. Most of the Q values obtained lie in an interval between about 20 and 70. Only for the Γ–X symmetry direction and TM polarized light, some exceptionally high values are obtained, which are not considered for the evaluation in order to avoid statistical deviation, such that the resulting mean Q value is more likely to be under-estimated than over-estimated. The Q values obtained for the Γ–X symmetry direction yield a mean value of 46 ± 4 for TM polarized light and of 43 ± 3 for TE polarized light. For the second symmetry direction, Γ–M, the mean Q values are 45 ± 4, and 45 ± 5 for TM and TE polarized light, respectively.

The four mean Q values for the two different symmetry directions and the two light polarizations hardly vary, such that we can estimate the quality factor of the leaky modes of the 2D PhC to be around 45. This Q factor is about two orders of magnitude lower than what is typically obtained for comparable, defect-free PhC slabs manufactured using other methods, such as electron-beam lithography [17]. The effect is probably intrinsic to the LIL manufacturing process that seems to produce short-range errors in the hole shape (as can also be seen by the slightly irregularly shaped holes in the SEM image). The periodicity, on the other hand, is entering the data as well due to the large probe beam diameter. The observed Q values thus form an upper limit also for long-range periodicity errors, which should be low as compared with other manufacturing methods, because in contrast to those, LIL does not require a displacement of the sample and is thus free of stitching errors.

4.4. Guided modes band structure

With the parameters used to fit the data from the reflectivity measurements (section 4.1), we can now calculate the dispersion of the guided modes, i.e. the modes under the light line based on a plane-wave simulation [27]. Figure 7 shows the so calculated band structure for TE polarized light [27,28], which is obtained with the same parameters as used before for the reflectivity spectra, i.e. a periodicity of 1 μm and a hole radius of 0.4 μm. In figure 7, the normalized frequency is plotted as a function of the normalized wavevector along a path connecting the high-symmetry points Γ–X–M–Γ. This path is sufficient to show all the minima and maxima of all bands [29] and thus allows for the identification of bandgaps, i.e. frequency intervals, which are free of guided modes. The modes are calculated along this path and displayed as solid black lines. The dispersion of light in air, the light line, forms a cone in this graph and is displayed as a solid grey line. In figure 7, one can identify several intervals under the light cone, which are free of guided modes. One of these bandgaps is of particular interest for nonlinear experiments, namely, the bandgap spanning the frequency range from 0.328 to 0.361, i.e. the wavelength range from 2.7 to 3 μm. This range corresponds to a bandgap for TE polarized light around a wavelength of 2.8 μm and of a width of about 10% of its centre wavelength. Close to this bandgap, the PhC guided modes show the strong anomalous dispersion in the MIR spectral range we were aiming at when designing this crystal.

The band structure is also completed for TM polarized light, which is displayed along a path connecting the high-symmetry points Γ–X–M–Γ in figure 8. The guided modes for TM polarized light, i.e. the modes lying under the light cone in figure 8, also show a gap, in the range of interest: a gap for light frequencies between 0.42 and 0.466, or for wavelengths in the range from 2.17 to 2.38 μm. We thus expect a bandgap for TM polarized light around a wavelength of 2.2 μm and of a width of about 8% of its centre wavelength.

For both polarizations, the 2D PhC thus offers a bandgap at photon energies, which are less than half the electronic bandgap of silicon, i.e. at wavelengths longer than 2.1 μm. In the vicinity of this bandgap, the PhC shows a strong anomalous dispersion in a material with a positive Kerr-coefficient, as it is required for spatio-temporal solitons to form. In conclusion, a prerequisite for performing nonlinear experiments is fulfilled with the fabrication of this PhC.

5. Summary and conclusion

In summary, we have presented the first, linear characterization of a square lattice PhC slab based on Si. The PhC has been designed to provide strong anomalous dispersion in the MIR wavelength range above 2.1 μm in order to enable the formation of spatio-temporal solitons and study nonlinear effects, and has been fabricated using LIL. We have obtained the energy against wave vector dispersion curves in the range from 1.9 to 2.8 μm by means of reflectance spectroscopy at oblique incidence and have, for the first time, determined the quality factors of the leaky modes observed for the PhC sample manufactured with LIL. From our results, it seems that LIL, in comparison with other commonly used processes, enables the manufacturing of large structures of rather poor short-range quality, but of excellent long (mm-) range periodicity.

The dispersion curves of the guided modes have been calculated, and the existence of a bandgap could be verified for both polarizations. In the vicinity of the bandgaps, regions of anomalous dispersion could be identified as required for nonlinear experiments in the MIR spectral region.

In conclusion, we have designed, manufactured and calculated the dispersion properties of a PhC slab using calculations complemented by specular reflectivity experiments. The highly nonlinear Kerr material with modified dispersion in the MIR should enable us to perform nonlinear experiments at high intensities of light, such as on the formation of spatio-temporal solitons, while the nonlinear, i.e. two-photon losses are reduced due to the low photon energies.

Acknowledgments

The authors acknowledge the financial support by the Dutch Stichting voor Fundamenteel Onderzoek der Materie (FOM), the Nederlandse Organisatie voor Wetenschappelijk Onderzoek (NWO) and the Deutsche Forschungsgemeinschaft (DFG). We thank Dr C Bostan, Dr H L Offerhaus and Dr M E Klein for stimulating discussions, and we thank R Hagen, R Arts, J Couperus, M Smithers, P Hartgers (LAC), F Ploegman (LAC) and the clean room staff of the MESA$^+$ Research Institute for technical support.

References

[1] Joannopoulos J D, Maede R D and Win J N 1995 *Photonic Crystals, Molding the Flow of Light* (Princeton: Princeton University Press)
[2] Yablonovitch E 1987 Inhibited spontaneous emission in solid-state physics and electronics *Phys. Rev. Lett.* **58** 2059–62
[3] John S 1987 Strong localization of photons in certain disordered dielectric superlattices *Phys. Rev. Lett.* **58** 2486
[4] Fan S, Winn J N, Devenyi A, Chen J C, Meade R D and Joannopoulos J D 1995 Guided and defect modes in periodic waveguides *J. Opt. Soc. Am.* B **12** 1267
[5] Raineri F, Cojocaru C, Raj R, Monnier P, Levenson A, Seassal C, Letartre X and Viktorovitch P 2005 Tuning a two-dimensional photonic crystal resonance via optical carrier injection *Opt. Lett.* **30** 64
[6] Leonard S W, van Driel H M, Schilling J and Wehrspohn R B 2002 Ultrafast band-edge tuning of a two-dimensional silicon photonic crystal via free-carrier injection *Phys. Rev.* B **66** 161102(R)
[7] Hache A and Bourgeois M 2000 Ultrafast all-optical switching in a silicon-based photonic crystal *Appl. Phys. Lett.* **77** 4089
[8] Fibich G and Ilan B 2004 Optical light bullets in a pure Kerr medium *Opt. Lett.* **29** 887
[9] Eisenberg H S, Morandotti R, Silberberg Y, Bar-Ad S, Ross D and Aitchison J S 2001 Kerr spatiotemporal self-focusing in a planar glass waveguide *Phys. Rev. Lett.* **87** 043902
[10] Vogelaar L, Nijdam W, Wolveren H A G M, Ridder R M, Segerink B, Flück E, Kuipers L and Hulst N F 2001 Large area photonic crystal slabs for visible light with waveguiding defect structures: fabrication with focused ion beam assisted laser interference lithography *Adv. Mater.* **13** 1551
[11] Goorjian P M and Silberberg Y 1997 Numerical simulations of light bullets using the full-vector time-dependent nonlinear Maxwell equations *J. Opt. Soc. Am.* B **14** 3253

[12] Kelly P L 1965 Self-focusing of optical beams *Phys. Rev. Lett.* **15** 1005
[13] Mollenauer L F, Stolen R H and Gordon JP 1980 Experimental observation of picosecond pulse narrowing and solitons in optical fibers *Phys. Rev. Lett.* **45** 1095
[14] Dinu M, Quochi F and Garcia H 2003 Third-order nonlinearities in silicon at telecom wavelengths *Appl. Phys. Lett.* **82** 2954
[15] SOITEC, Parc Technologique des Fontaines, 38190 Bernin, France
[16] Prodan L, Euser T G, Wolferen H A G M, Bostan C, Ridder R M, Beigang R, Boller K J and Kuipers L 2004 Large-area two-dimensional silicon photonic crystals for infrared light fabricated with laser interference lithography *Nanotechnology* **15** 639
[17] Krauss T, Song Y P, Thoms S, Wilkinson C D W and De La Rue R 1994 Fabrication of 2-D photonic band gap structures in GaAs/AlGaAs *Electron. Lett.* **30** 1444
[18] Chelnokov A, Wang K, Rowson S, Garoche P and Lourtioz J M 2000 Near- infrared Yablonovite-like photonic crystals by focus ion beam etching of macroporous silicon *Appl. Phys. Lett.* **77** 2943
[19] Bogaerts W, Wiaux V, Taillaert D, Beckx S, Luyssaert B, Bienstman P and Baets R 2002 Fabrication of photonic crystals in silicon-on-insulator using 248 nm deep UV lithography *IEEE J. Sel. Top. Quantum Electron.* **8** 928
[20] Galli M, Bajoni D, Belotti M, Paleari F, Patrini M, Guizzetti G, Gerace D, Agio M, Andreani L C, Peyrade D and Chen Y 2005 Measurement of photonic mode dispersion and linewidths in silicon-on-insulator photonic crystal slabs *IEEE J. Sel. Areas Commun.* **23** 1402
[21] Astratov V N, Culshaw I S, Stevenson R M, Whittaker D M, Skolnick M S, Krauss T F and De La Rue R M 1999 Resonant coupling of near-infrared radiation to photonic band structure waveguides *J. Lightwave Technol.* **17** 2050
[22] Pacradouni V, Mandeville W J, Cowan A R, Paddon P, Young J F and Johnson S R 2000 Photonic band structure of dielectric membranes periodically textured in two dimensions *Phys. Rev.* B **62** 4204
[23] Berger T and Brookner E 1967 Practical design of infrared detector circuits *Appl. Opt.* **6** 1189
[24] Patrini M, Galli M, Marabelli F, Agio F, Andreani L C, Peyrade D and Chen Y 2002 Photonic bands in patterned silicon-on-insulator waveguides *IEEE J. Quantum Electron.* **38** 885
[25] Fano U 1961 Effects of configuration interaction on intensities and phase shifts *Phys. Rev.* **124** 1866
[26] Mies F H 1968 Configuration interaction theory. Effects of overlapping resonances *Phys. Rev.* **175** 164
[27] Johnson S G and Joannopoulos J D 2001 Block-iterative frequency-domain methods for Maxwell's equations in a planewave basis *Opt. Express* **8** 173
[28] Fan S H and Joannopoulos J D 2002 Analysis of guided resonances in photonic crystal slabs *Phys. Rev.* B **65** 235112
[29] Ochiai T and Sakoda K 2001 Nearly free-photon approximation for two dimensional photonic crystal slabs *Phys. Rev.* B **64** 045108